NEW QUADRANGULAR SHELL ELEMENT IN SAFIR

Didier TALAMONA – Jean-Marc FRANSSEN
Univ. of Liège, SPEC, 1 Chemin des Chevreuils, 4000 Liège 1, Belgium
d.talamona@ulg.ac.be – jm.franssen@ulg.ac.be

Abstract

SAFIR is a finite element program for the thermal and mechanical analysis of structures submitted to fire. Usually, thermal calculations are run in a first step to determine the temperatures in the structure subjected to fire. In a second step, mechanical analyses are performed to determine the time when collapse will occur.
In case of mechanical analysis, different elements are available in SAFIR : truss, beam and shell.
The shell element in SAFIR was a triangle with 6 nodes. It gave good results except in case of 'membrane bending' where the answer was too stiff. Furthermore, this element was heavy to use because 3 nodes had 6 DOF and the 3 others had only 1 DOF.
In order to improve SAFIR, it has been decided to introduce a new quadrangular element to eliminate the over-stiffness of the triangular element in case of 'membrane bending'. This element has been taken from the room temperature program FINELG (developed by de Ville at the University of Liège and the Bureau d'Etudes Greisch).
In a first step, this element has been introduced in SAFIR with success. The material law has then been modified to perform calculations under fire conditions. Calculations may be performed using bi-linear or elliptical hardening (according to ENV 1993-1-2). The 2 D yield surface is the Von Mises surface. The ultimate strength, the Young modulus, the limit of proportionality and the thermal expansion also follow the recommendations of ENV1993-1-2.
Some validation examples are presented: a Z-Shaped cantilever, an hemispherical shell and Lee's frame are treated.

Keywords : *SAFIR, finite element, shell, thermal*

FORMULATION OF THE SHELL ELEMENT

This element has been taken (and adapted) from the program Finelg developed by de Ville at the University of Liège and the Bureau d'Etudes Greisch [1, 2, 3, 4, 5].

Reference configuration

For this quadrangular element the *z* axis is obtained as follows:

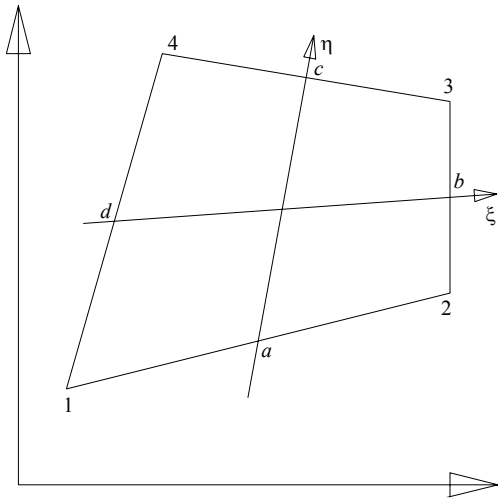

Figure 1 : Reference configuration.

a, *b*, *c* and *d* are the middle edge points, not necessarily located in one plane. The *z* axis is defined as:

$$\underline{z} = \frac{(\underline{db} \wedge \underline{ac})}{\left\| \underline{db} \wedge \underline{ac} \right\|} \tag{1}$$

Another way to define the *z* axis could be to find the best plane reference for the element :

$$w_0 = \alpha_1 + \alpha_2 x + \alpha_3 y \tag{2}$$

It can be shown that, if the coefficients α_2 and α_3 are chosen in such a way that the orientation of the reference plane minimizes the slopes between the element and the plane, then the *z* axis defined by eq. 1 is perpendicular to the plane. This proves that eq. 1 minimizes also the slopes.

In eq. 2, α_1 is still undetermined. It will be chosen in such a way that the plane of reference goes through the center of gravity of the quadrangle.

As it will be seen later, the membrane strains are not complete polynomials, so the results will be dependent on the choice of the *x*, *y* local axis. The angle between the *x* axis and $\underline{bd}$ is imposed to be equal to the angle between $\underline{ac}$ and the *y* axis. This determines the choice of the *x*, *y* axis. For a rectangular element, this gives local axes parallel to the edges.

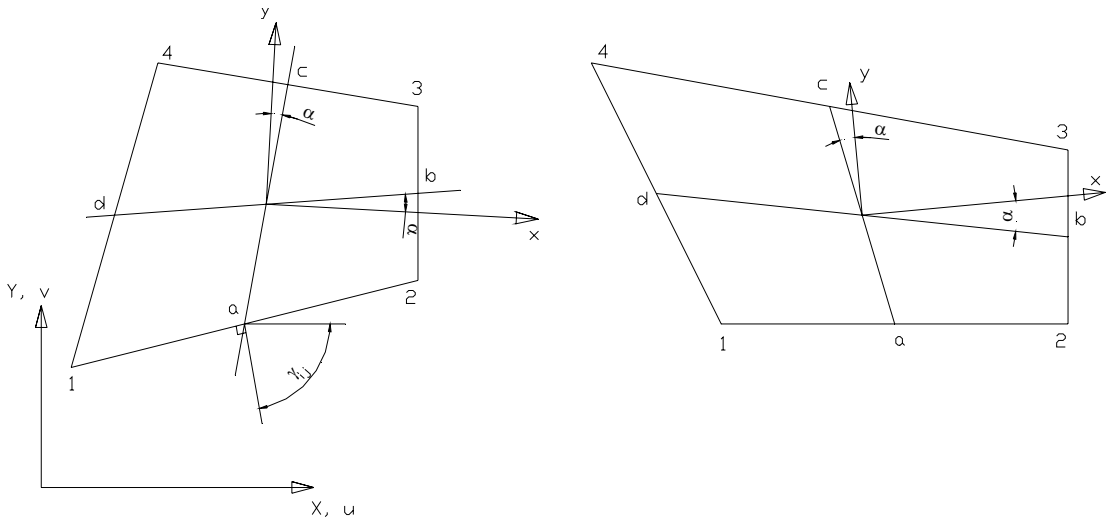

Figure 2 : Local axes *x* and *y*.

The membrane behavior

The classical quadratic membrane displacement field is enlarged to cubic degree by means of cubic (along ξ and η) functions and constants A_{ij}. It is the same development as ALLMAN [6] for a triangle element.

$$u = \frac{1}{4}\left[\sum_{k=1}^{4}\left(1+\xi\xi_k\right)\left(1+\eta\eta_k\right)u_k + \sum_{sides}\phi_{ij}l_{ij}\cos\gamma_{ij}\left(\omega_j-\omega_i\right) + \sum_{sides}\psi_{ij}l_{ij}\cos\gamma_{ij}\;A_{ij}\right] \tag{3}$$

$$v = \frac{1}{4}\left[\sum_{k=1}^{4}\left(1+\xi\xi_k\right)\left(1+\eta\eta_k\right)v_k + \sum_{sides}\phi_{ij}l_{ij}\sin\gamma_{ij}\left(\omega_j-\omega_i\right) + \sum_{sides}\psi_{ij}l_{ij}\sin\gamma_{ij}\;A_{ij}\right]$$

$$\phi_{12} = \frac{1}{16}\left(1-\xi^2\right)\left(1-\eta\right) \qquad \psi_{12} = \frac{1}{8}\left(1-\xi^2\right)\left(1-\eta\right)\xi\eta^2$$

$$\phi_{23} = \frac{1}{16}\left(1+\xi\right)\left(1-\eta^2\right) \qquad \psi_{23} = \frac{1}{8}\left(1+\xi\right)\left(1-\eta^2\right)\xi^2\eta \tag{4}$$

$$\phi_{34} = \frac{1}{16}\left(1-\xi^2\right)\left(1+\eta\right) \qquad \psi_{34} = -\frac{1}{8}\left(1-\xi^2\right)\left(1+\eta\right)\xi\eta^2$$

$$\phi_{41} = \frac{1}{16}\left(1-\xi\right)\left(1-\eta^2\right) \qquad \psi_{41} = -\frac{1}{8}\left(1-\xi\right)\left(1-\eta^2\right)\xi^2\eta$$

$$l_{ij} = \sqrt{\left(x_j-x_i\right)^2+\left(y_j-y_i\right)^2} \tag{5}$$

$$A_{ij} = \frac{\omega_i+\omega_j}{2} + \frac{B_{ij}+B_{ji}}{2} \tag{6}$$

ω_i is the rotation at node i and ω_j is the rotation at node j.
γ_{ij} is the direction of the outward normal along the edge ij.
If i = 1 and j = 2 then B_{ij} and B_{ji} are equal to (for the complete definition see [7]):

$$B_{12} = \frac{1}{4 J_1} \left(x_{41}\, u_1 + x_{14}\, u_2 + y_{41}\, v_1 + y_{14}\, v_2 \right) \tag{7}$$

$$B_{21} = \frac{1}{4 J_2} \left(x_{23}\, u_1 + x_{32}\, u_2 + y_{23}\, v_1 + y_{32}\, v_2 \right) \tag{8}$$

$$J_1 = \frac{1}{4} \left(x_{21}\, y_{41} - x_{41}\, y_{21} \right) \tag{9}$$

$$J_2 = \frac{1}{4} \left(x_{21}\, y_{32} - x_{32}\, y_{21} \right) \tag{10}$$

The function ψ_{ij} are chosen so as to be orthogonal to ϕ_{ij} with respect to integration over the quadrangle.

To improve the convergence, the shear strains are assumed to be constant over the element. After some calculation, the following equations are found:

$$\begin{aligned}
\varepsilon_x &= \frac{1}{8J}\left[\left(y_{42} u_{31} - y_{31} u_{42} \right) + \xi \left(y_{21} u_{43} - y_{43} u_{21} \right) + \eta \left(y_{41} u_{32} - y_{32} u_{41} \right) \right] \\
\varepsilon_y &= \frac{1}{8J}\left[\left(v_{42} x_{31} - v_{31} x_{42} \right) + \xi \left(v_{21} x_{43} - v_{43} x_{21} \right) + \eta \left(v_{41} x_{32} - v_{32} x_{41} \right) \right] \\
\bar{\gamma} &= \frac{1}{8J_0}\left[\left(u_{42} x_{31} - u_{31} x_{42} \right) + \left(y_{42} v_{31} - y_{31} v_{42} \right) \right]
\end{aligned} \tag{11}$$

J is the determinant of the Jacobian matrix, J_0 is the value of J at $\xi = \eta = 0$ and x_{31} is $x_3 - x_1$

Flexural behavior

The formulation used is a Discrete Kirchhoff theory Quadragular (DKQ). This element is fully described in [8, 9, 10, 11]. The principle of this element will be briefly recalled here. The presentation is slightly different from the one given in [8, 9, 10].

The out-of-plane displacement and the rotations are parabolic over each side:

$$w = \sum_{i=1}^{8} N_i w_i \qquad \beta_x = \sum_{i=1}^{8} N_i \theta_{yi} \qquad \beta_y = \sum_{i=1}^{8} N_i \theta_{xi} \tag{12}$$

N_i are the shape functions and they depend on the parametric coordinates ξ and η.
Along the side i, the out-of-plane displacement is given by:

$$w = -\xi \frac{\left(1-\xi\right) w_A}{2} + \left(1-\xi^2\right) w_C + \frac{\xi \left(1+\xi\right) w_B}{2} \tag{13}$$

w_A, w_B and w_C are the normal displacements along z axis normal to xy plane (at the points A, B, and C). If we look to one edge of the element, for example the edge from node 1 to node 2, the node 1 is called A, the node 2 is called B and the middle point is called C, see Figure 3.

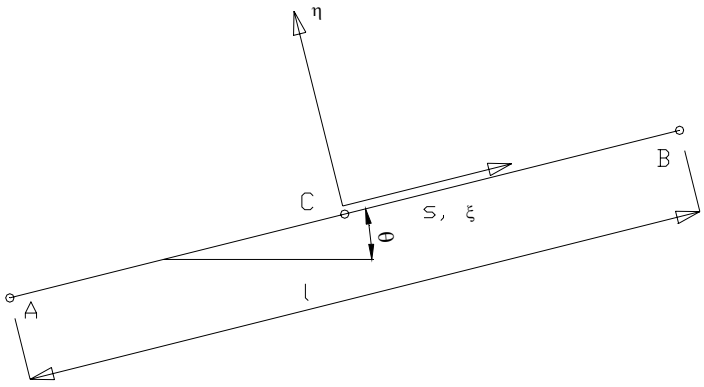

Figure 3 : Local axis on one side.

The contribution of the shear strain energy is neglected.
To reproduce thin plate theory, the Kirshhoff condition is imposed at selected points. In this element, the Kirshhoff constraints are imposed along the edges. The shear strain γ_{sz} at each of the two-point Gauss integration points along the sides is set to zero. Or, which is the same, weighted averages of the shear strain are set to zero:

$$\int_l \gamma_{sz}\, ds = 0 \qquad \int_l \gamma_{sz}\, s\, ds = 0 \tag{14}$$

Moreover, the rotation around the side θ_s is imposed to vary linearly.

$$w_{,s} = \frac{-(1-2\xi)w_A + 4\xi w_C + (1+2\xi)w_B}{l} \tag{15}$$

General features

The thickness is constant over the element.

The integration on the surface is performed with a 2 x 2 points Gauss scheme. The integration on the thickness is performed with a Gauss scheme using a user defined number of points.

The temperature varies on the thickness of the element and comes from a thermal SAFIR analysis which has to be performed before the mechanical analysis. The temperature distribution on the thickness is the same at every surface point of integration.

MATERIAL PROPERTIES

A steel material law has been introduced in SAFIR to perform calculations at elevated temperature. Plane stress relationships have been introduced for isotropic materials.
The thermal strain is taken into account in SAFIR according to ENV 1993-1-2 and it is supposed to be hydrostatic (i.e. $\varepsilon_{thxx} = \varepsilon_{thyy} = \varepsilon_{th}$).
Two types of hardening relationships have been introduced in SAFIR : linear and elliptical.
For linear hardening, the input data are E_0, E^* and f_y, see figure 4.

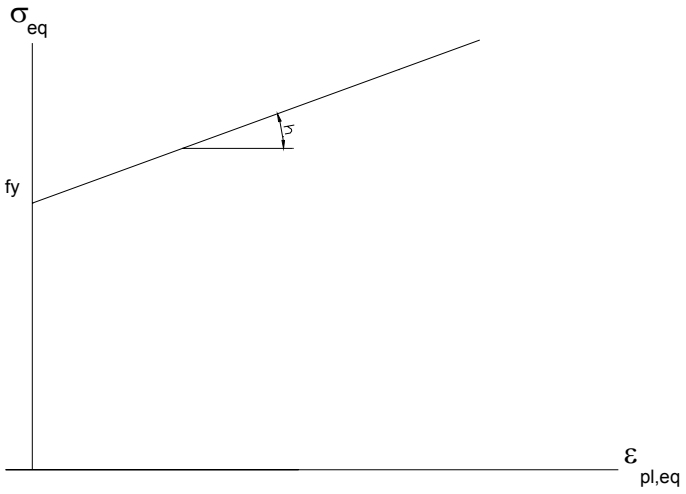

Figure 4 : Linear hardening

With : $h = \dfrac{E * E^*}{E - E^*}$ (16)

The elliptical law is not exactly equal to the function defined as the stress-strain relationship in the EC3. This is because EC3 defines the relationship in the σ-ε plane, whereas the present law is defined in the σ_{eq}-$\varepsilon_{pl,eq}$ plane (figure 5).

The hardening function is defined as:

$$\sigma_{eq} = f_p \sqrt{b\left[1 - \frac{\left(\varepsilon_{pl,eq} - a\right)^2}{a^2}\right]} \qquad (17)$$

$a = 0.02 - f_y / E$ $\qquad$ $b = f_y - f_p$

f_y : Ultimate strength, $\qquad$ f_p : Limit of proportionality, $\qquad$ $\varepsilon_{pl,eq}$: Equivalent plastic strain

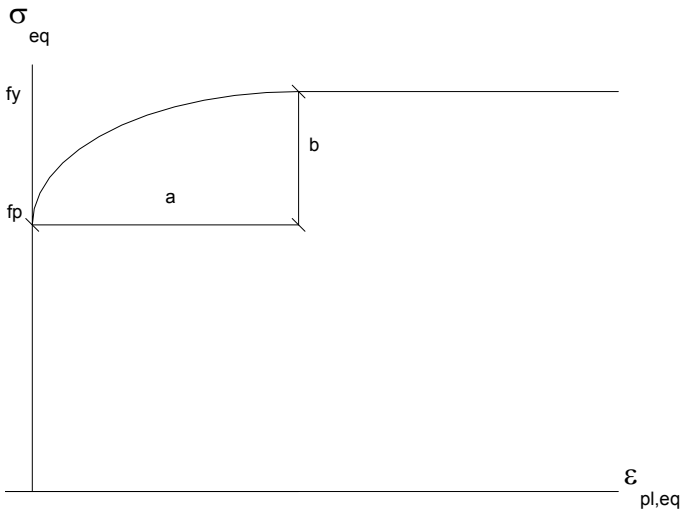

Figure 5 : Elliptic hardening

Evolution of the parameters at elevated temperatures

The following equations are used to calculate the Yield strength, the Young modulus, Tangent modulus and the Proportional limit at elevated temperature:

$\sigma_{y,\theta} = k_{y,\theta}\,\sigma_{y,20}$ $\quad E_\theta = k_{E,\theta}\,E_{20}$ $\quad \sigma_{p,\theta} = k_{p,\theta}\,\sigma_{y,20}$ $\quad E^*_\theta = k_{E,\theta}\,E^*_{20}$

The coefficients $k_{y,\theta}$, $k_{E,\theta}$ and $k_{p,\theta}$ are defined in ENV 1993-1-2.

Algorithmic strategy

A point of the structure at the time '*t*' (step *n*) is represented by **A** on figure 6. It is defined by:

t_n : time
T_n : temperature at the time t_n
σ_{eq} - $\varepsilon_{pl,eq}$: the hardening function, depending on T_n
$\varepsilon_{pl,eq,n}$: the equivalent plastic strain
$\{\sigma_n\}$: the stress vector
$\{\varepsilon_{tot,n}\}$: the total strain vector
$\{\varepsilon_i\}$: the initial strain vector
$\{\varepsilon_{th,n}\}$: the thermal strain vector
$\{\varepsilon_{m,n}\}$: the mechanical strain vector
$\{\varepsilon_{pl,n}\}$: the plastic strain vector
$[D_n]$: elastic constitutive matrix

If the initial strain $\{\varepsilon_i\}$ and the thermal strain $\{\varepsilon_{th,n}\}$ are subtracted from the total strain $\{\varepsilon_{tot,n}\}$, the mechanical strain $\{\varepsilon_{m,n}\}$: is obtained from

$$\{\varepsilon_{m,n}\} = \{\varepsilon_{tot,n}\} - \{\varepsilon_i\} - \{\varepsilon_{th,n}\} \tag{18}$$

It is also possible to calculate the plastic strain, i.e. the mechanical strain that would exist in the structure if it was elastically unloaded. This is point **B** on figure 6. Note that the unloaded structure is not equivalent to the initial structure (non deformed). The equation is

$$\{\varepsilon_{pl,n}\} = \{\varepsilon_{m,n}\} - [D_n]^{-1}\{\sigma_n\} \tag{19}$$

When the temperature changes from T_n to T_{n+1}, it is possible to determine the new Von Mises surface which corresponds to the new hardening parameter, assuming that the plastic strain is not affected by the variation of temperature, i.e. the plastic strain is not modified from the end of step *n* to the beginning of step *n+1*.

In the algorithm used by SAFIR, it is supposed that the structure is 'locked' at the first iteration of each time step, i.e.

$$\{\varepsilon^J_{tot,n+1}\} = \{\varepsilon_{tot,n}\} \tag{20}$$

As the thermal strain is modified by the variation of temperature, the 'mechanical' strain changes accordingly:

$$\{\varepsilon^J_{m,n+1}\} = \{\varepsilon_{tot,n}\} - \{\varepsilon_i\} - \{\varepsilon_{th,n+1}\} \tag{21}$$

It is now represented by the point **D** on figure 6. The segment **A-D** represents the increase of thermal strain from temperature T_n to T_{n+1}. As the thermal strain is hydrostatic, this part is inclined at 45° on figure 6 b.

For each iteration the calculation will start from the unloaded structure (point **B**). The strain increment to be applied from the unloaded state is given by:

$$\{\Delta\varepsilon^1\} = \{\varepsilon^1_{m,n+1}\} - \{\varepsilon_{pl,n}\} \quad (22)$$

The classic plasticity theory is applied at temperature T_{n+1} in order to load the structure from point **A** to point **D**, see figure 6. The stress $\{\sigma^1_{n+1}\}$ and the new tangent matrix $[D^1_{t,n+1}]$ are computed. The return mapping algorithm, and Euler backward algorithm for the integration of the plastic strain, established at ambient temperature are used here.

Of course, the stresses obtained in the structure after the first iteration are not in equilibrium and they generate out of equilibrium forces in the structure which, using the new tangent stiffness matrix allow the calculation of displacement increments and their corresponding strain increments $\{\Delta\varepsilon^{1\text{-}2}\}$

At next iteration, the strain increment to be applied from the unloaded state is:

$$\{\Delta\varepsilon^2\} = \{\Delta\varepsilon^1\} + \{\Delta\varepsilon^{1\text{-}2}\} \quad (23)$$

In fact, in the calculations, the temperature does not vary during a time step.

When the equilibrium is finally reached, if the point **D** is outside the yield surface calculated at the beginning of the time step T_{n+1}, the hardening has increased and this is taken into account by updating the plastic strain and the equivalent plastic strain of the yield surface.

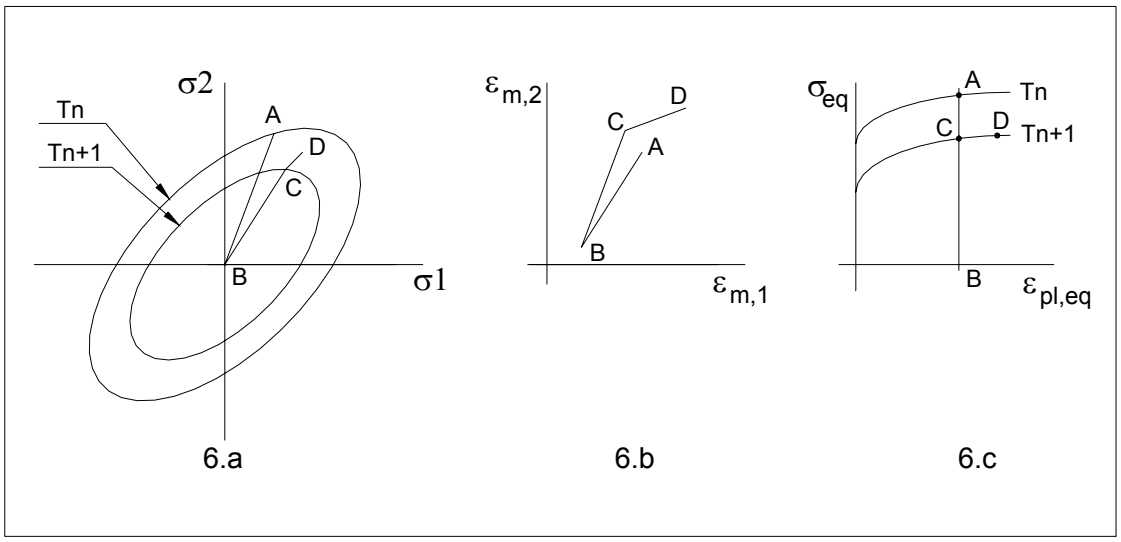

Figure 6 : First iteration of a time step in plastic behavior.

NUMERICAL TEST

Response of a Z-shaped cantilever

The structure is a Z-shaped cantilever subjected to a transverse end load (fig. 7).

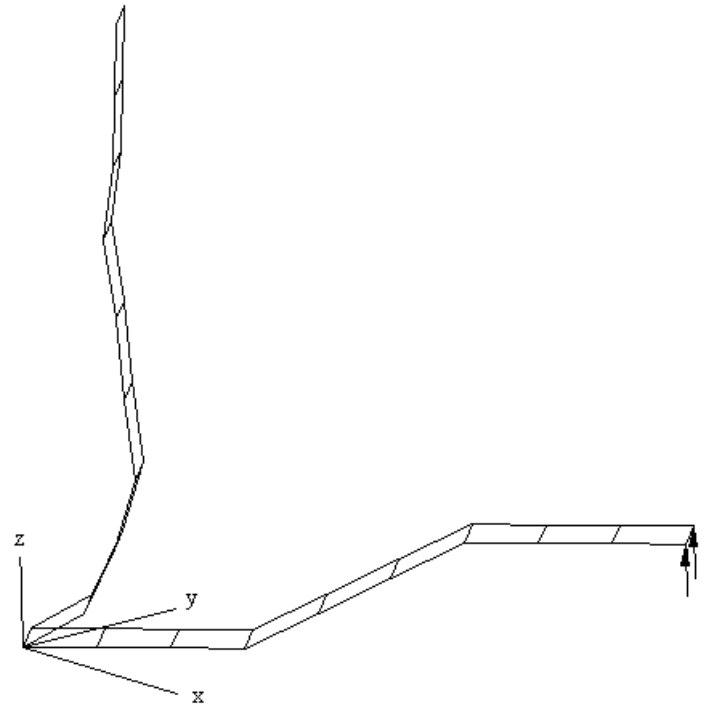

Figure 7 : Initial geometry and deformed shape for a load of 4000.

The solution given in reference [12] is based on nine equal sized element. The structure is oriented at 45° from the x-z plane to activate all three translation and rotations in the element formulation.
The beam is divided into 3 equal parts (each part is meshed with 3 elements). The 2 parts parallel to the x-y plane have a length of 60 and a width of 20. The middle part (inclined) has also a length of 60 and an elevation of 30 in the z-direction, the width is 20. The thickness of the beam is 1.7 (consistent units).
All the six degrees of freedom are restrained at one end and two concentrated nodal forces are applied in the positive z-direction at the other end. The load is increased up to 4000 with a step of 10.
The material is elastic, the Young modulus is equal to 2.0×10^5 and poison's ratio is equal to 0.3. This problem is solved at ambient temperature (20°C).

Two calculations have been performed, the first one "Deflec-Z-Safir" with a load increment of 10, to check that SAFIR gives the same continuous curve as the one given by NAFEMS. The second one with a larger load increment of 500 to check whether SAFIR is able to manage large steps. It can be seen on fig. 7 (displacements not amplified) and 8 that the new element introduced in SAFIR gives good results in case of bending with large geometric non linear behavior. The results obtained for a load step of 500 are also very good even if the first point is a little bit too high compared to the two other curves. It has to be realized that a displacement of nearly 125 has been accommodated within one single step.

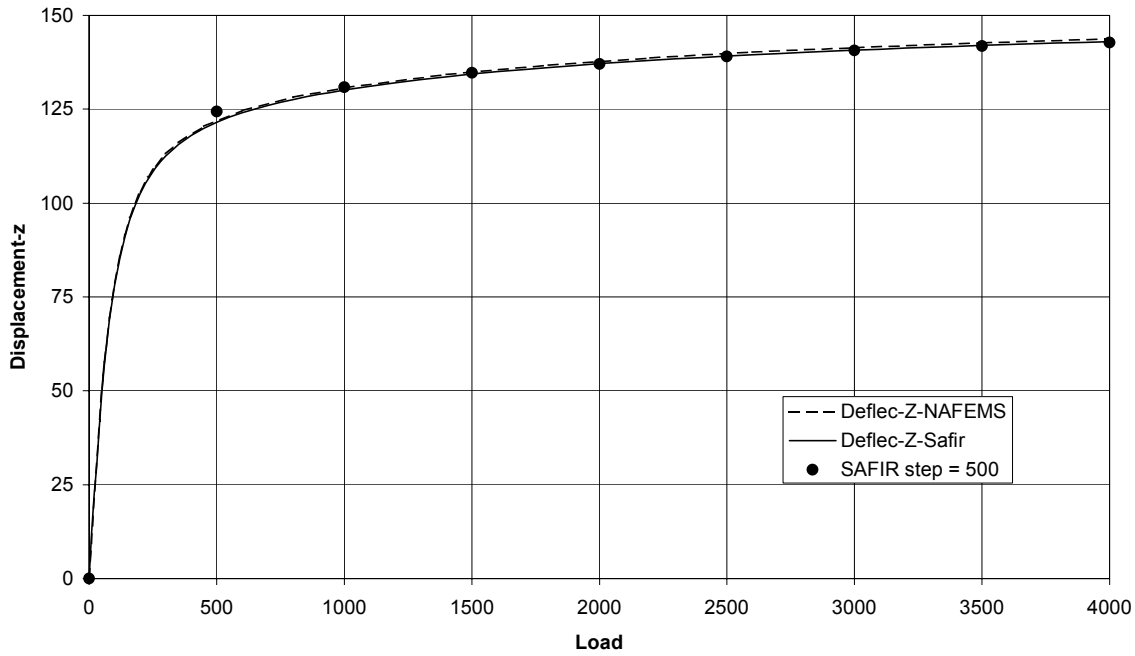

Figure 8 : Load/Displacement.

Hemispherical shell

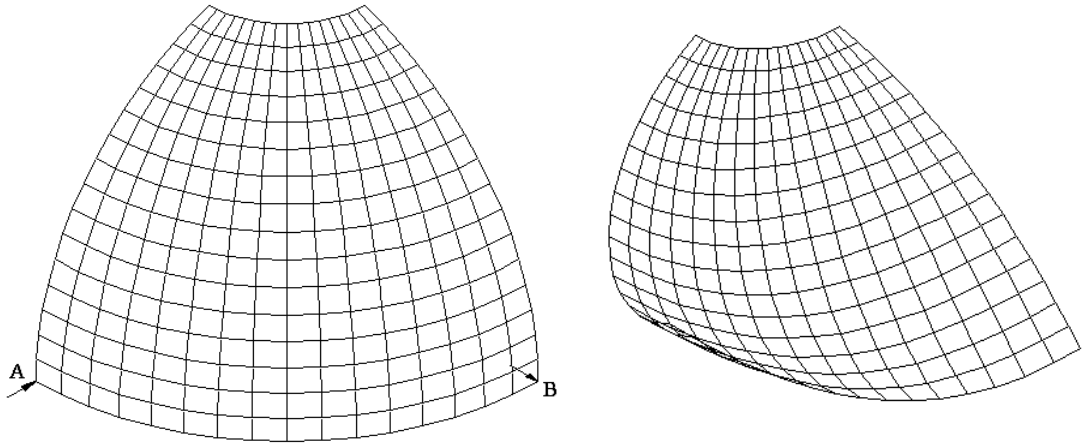

Figure 9 : Hemispherical shell.

The finite element mesh is shown on figure 9. 1/8 of the sphere [12] has been meshed with 16x16 quadrilateral elements. The units are consistent.
The radius of the sphere is 10 and the thickness is equal to 0.04.
The following symmetrical boundary condition have been used:
Symmetry on the plane y = 0

$$U_y = \theta_x = \theta_z = 0$$

Symmetry on the plane x = 0

$U_x = \theta_y = \theta_y = 0$

To prevent the rigid body mode in the z-direction, the point A was restrained to have x-translations only, i.e. $U_z = 0$

Inward and outward diametral point loads were applied as concentrated nodal forces at locations A and B respectively. The loads are increased up to a maximum of 100.

The material is elastic, the Young modulus is equal to 6.825×10^7 and poison's ratio is equal to 0.3. This problem is solved at ambient temperature (20°C).

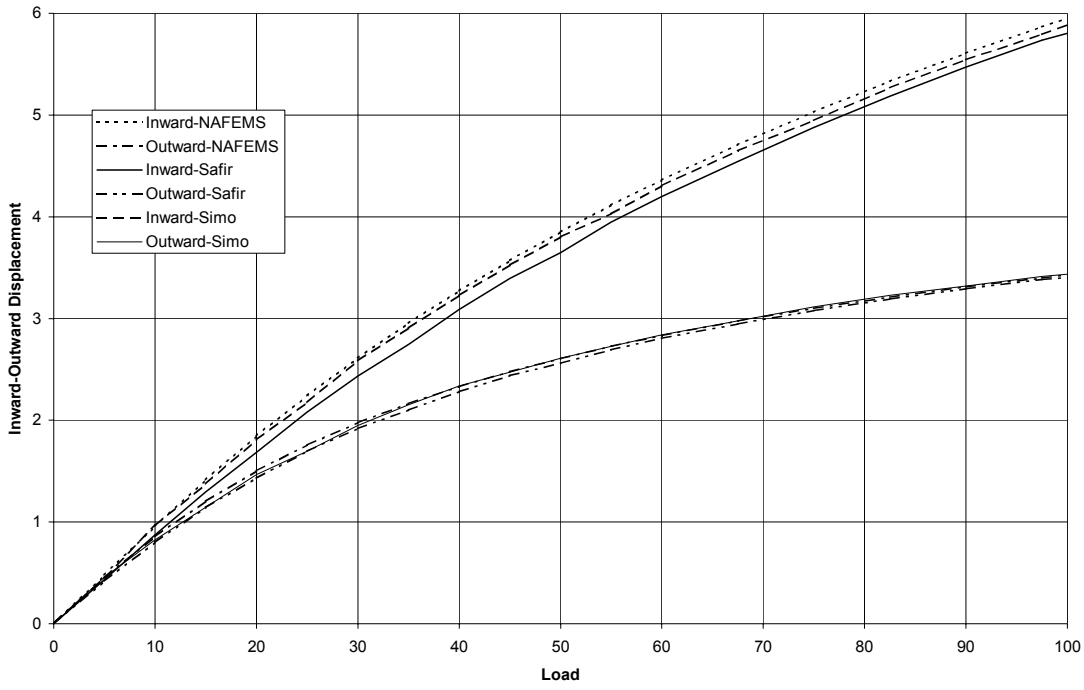

Figure 10 : Inward and outward displacements.

This problem tests the performance of the geometric non-linear formulation for shells under membrane, bending and twisting actions. It can be seen (fig. 10) that SAFIR gives good results in case of large rotations and deflections. For the inward displacement, SAFIR is stiffer than the results obtain by NAFEM [12], but the results are close to the one obtained by Simo. This test confirms that there is no membrane locking in the element.

Note : Simo has performed his calculation for a load going from 0 up to 60. NAFEMS has extrapolated the values up to 100.

Lee's Frame

The finite element mesh is shown on figure 11. The vertical and the horizontal members have a length of 120. Two meshes have been used to check the behavior in case of bending and in case of 'membrane bending'.

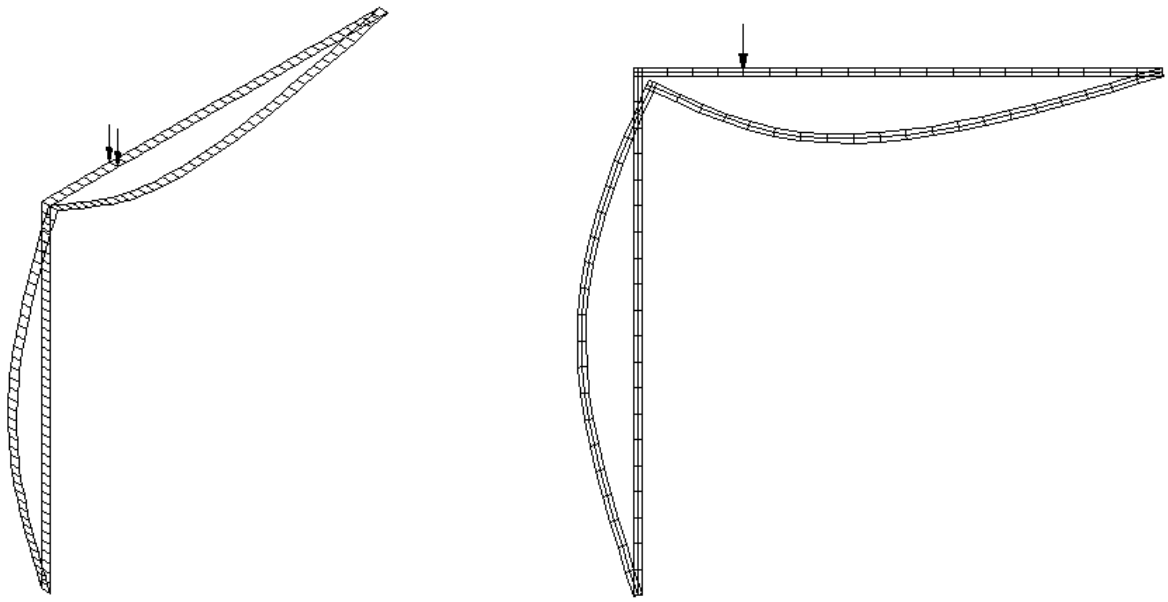

Figure 11 : Lee's frame

At the ends of the frame, the following displacements have been locked:

$$U_x = U_y = U_z = \theta_x = \theta_z = 0$$

The units are consistent. The cross-section of the beam is equal to 6 and the inertia is equal to 2. The elements are divided into 8 layers.

Ambient temperature

A vertical load is applied at a distance of 96 of the top right edge and it is increased until collapse.

The material is elastic, the Young modulus is equal to 720 and poison's ratio is equal to 0.3.

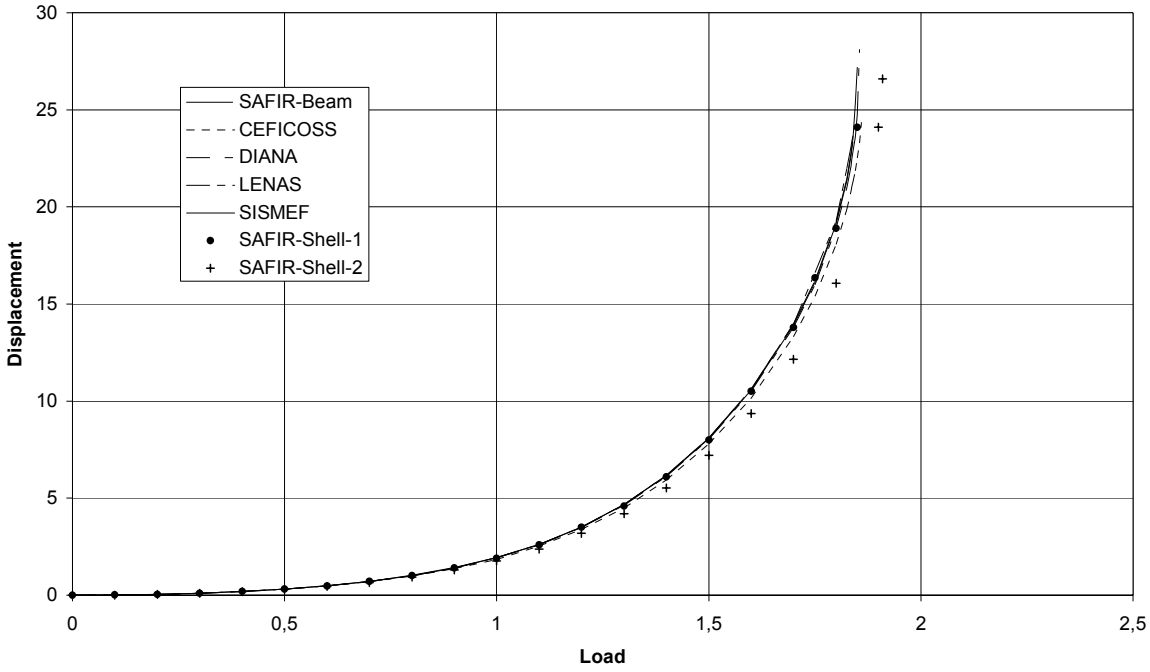

Figure 12 : Horizontal displacement versus load.

A comparison with the results of some beam elements [13] has been performed. It can be seen (fig. 12) that in case of bending (SAFIR-Shell -1) SAFIR gives results close to the been element. In case of "membrane bending" (SAFIR-Shell-2) the element is a little bit too stiff, but the mesh used here is very crude (2 elements on the depth of the beam).

Elevated temperature

A vertical load of 0.2 is applied to the structure at a distance of 96 from the right top edge. The temperature is uniform in the structure and it is increased until collapse.
The elliptic hardening is used, the Young modulus is equal to 720, the yield stress is equal to 3.0 and poison's ratio is equal to 0.3. The material properties decrease with temperature according to ENV 1993-1-2.
A comparison with some beam elements [13] has been performed under fire condition. It can be seen (fig. 13) that in case of bending (SAFIR-Shell-1) SAFIR gives results close to the beam element. In case of "membrane bending" (SAFIR-Shell-2) the results is a little bit higher than the results provided by the other elements. It has to be highlighted that the integration of plasticity on the depth of the beam is performed only at 4 integration points (2 in each of the 2 elements used in the discretisation).
This example shows that the new element takes correctly into account the thermal elongation and the stress-strain relationship according to EC3.

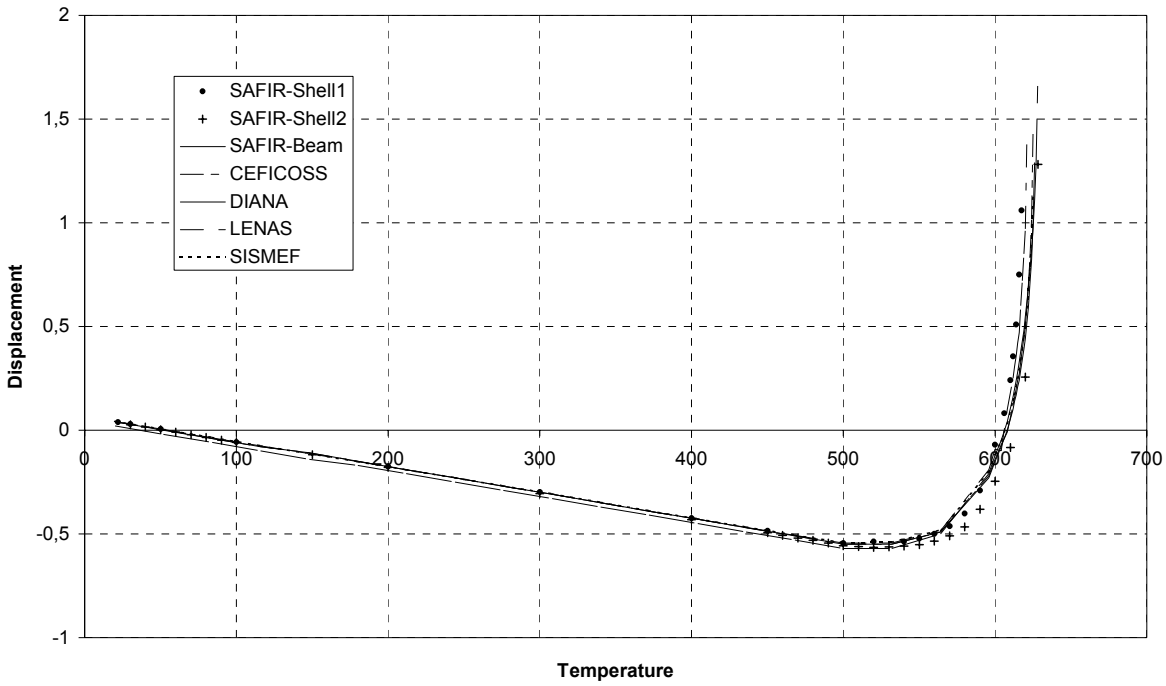

Figure 13 : Horizontal displacement versus temperature

H rolled profile

Calculations have been performed on a S355 HE 300 AA+. The length of the beam is 1 m. The boundary conditions are defined as follow:

First end : All the nodes are locked on the longitudinal displacement and all the rotations. The lateral displacement is locked at all the nodes on the web and all the displacements are locked at the point in the middle of the web.

Second end : All the nodes have an imposed longitudinal displacement in compression and all the rotations are locked. The lateral displacement is locked at all the nodes on the web and all the displacements are locked at the point in the middle of the web.

The temperature is uniform in the structure and it is increased in the same time as the displacement is increased.

An initial sinusoidal imperfection of 10 mm is imposed on the web and the flanges (fig. 14).

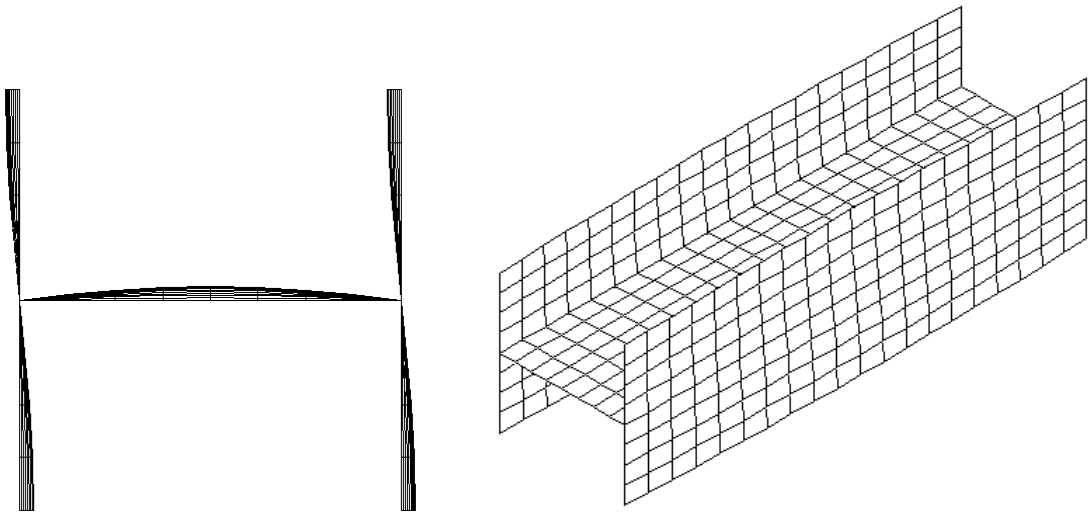

Figure 14 : Initial geometry of the H profile

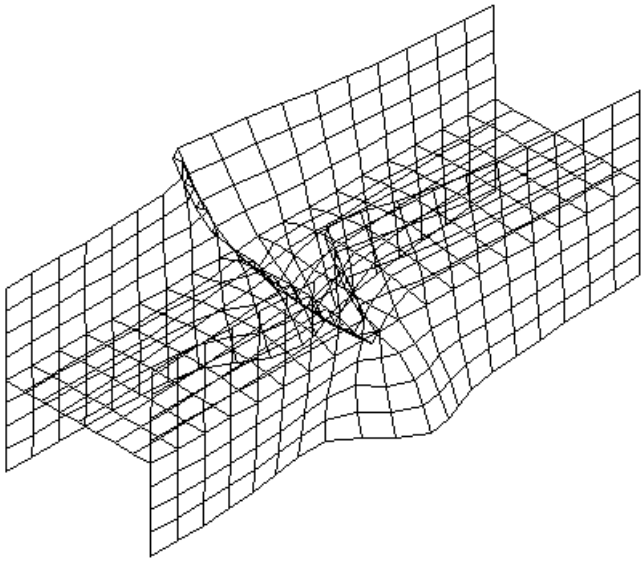

Figure 15 : Deformation of the H profile at the last converged step

In this structure, the stress is function of the imposed longitudinal displacement and the thermal strain (restrained). As the temperature and the displacement are increased at the same time collapse occurred when the temperature in the structure reach 42°C and the longitudinal displacement is equal to 1.8 mm. The ratio between the maximum load applied to the structure and the theoretical crushing compressive load is equal to 0.92. As the calculation has been performed with imposed displacement post-critical behavior can be study. Figure 15 shows the deformation of the beam at the last converged step (displacements not amplified) . It can be seen that large deformations have been obtained in the middle of the beam. The temperature in the structure at this moment is 888°C and the imposed displacement is equal to 72 mm.

CONCLUSION

After a brief description of the new quadrangular shell element introduced in SAFIR and the new material properties, some calculations have been performed to validate this element.
The z-shape cantilever show that the element can be subjected to large geometric non-linear behavior. The hemispherical shell and the calculation performed on Lee's frame at ambient temperature show that this element is not subjected to membrane locking.
Lee's frame at elevated temperature demonstrate that the material properties from EC3 have successfully been introduced in SAFIR in case of plane stress relationship and that the thermal elongation is taken into account.
To complete the validation of this element, more calculations have to be done on benchmark tests at elevated temperature and some comparison with experimental tests have to be performed.

ACKNOWLEDGEMENT

This work is supported by the European Commission through the *Marie Curie* fellowship granted to the first author (contract number ERBFMBICT983336). Nathalie Nicoletti's help in setting up the application form is appreciated.

REFERENCES

[1] FINELG – Nonlinear Finite Element Analysis Program – User's Manual Version 6.2 – Feb. 1984.

[2] Jetteur Ph. – Non-Linear Shell Elements Based On Marguerre Theory – IREM Internal Report 85/5 – Swiss Federal Institute Of Technology, Lausanne, Switzerland, Dec. 1985.

[3] Jetteur Ph. – A Shallow Shell Element With In-Plane Rotational Degrees Of Freedom – IREM Internal Report 86/3 – Swiss Federal Institute Of Technology, Lausanne, Switzerland, March 1986.

[4] Jetteur Ph. – Improvement Of The Quadrangular "JET" Shell Element For a Particular Class Os Shell Problems – IREM Internal Report 87/1 – Swiss Federal Institute Of Technology, Lausanne, Switzerland, Feb. 1987.

[5] Jammei S., Frey F., Jetteur Ph. – Elément Fini De Coque Mince Non-Linéaire à Six Defrés De Liberté par Noeud – IREM Internal Report 87/10 – Swiss Federal Institute Of Technology, Lausanne, Switzerland, Nov. 1987.

[6] Allman D.J. – A Compatible Triangular Element Including Vertex Rptations For Plane Elastic Analysis – Comput. Struct., Vol. 19, 1984, pp 1-8.

[7] Jaamei S. – "JET" Thin Shell Finite Element With Drilling Rotations – IREM Internal Report 88/7 – Swiss Federal Institute Of Technology, Lausanne, Switerland, July 1988.

[8] Idelsohn S.. – Analyses Statique et Dynamique Des Coques Par La Méthode Des Eléments Finis – Ph.D. thesis, Liège, 1974.

[9] Batoz J.L., Bathe K.J., Ho L.W. – A Study Of Three Node Triangular Plate Bending Elements – Int. J. Num. Meth. Eng., Vol. 15, pp. 1771-1812, 1980.

[10] Batoz J.L. – An Explicit Formulation For An Efficient Triangular Plate Bending Element – Int. J. Num. Meth. Eng., Vol. 18, pp. 1077-1089, 1982.

[11] Batoz J.L., Ben Tahar M. – Evaluation Of A New Quadrangular Thin Plate Bending Element – Int. J. Num. Meth. Eng., Vol. 18, pp. 1655-1677, 1982.

[12] Prinja N.K., Clegg R.A. – Assembly Benchmark Tests For 3-D Beams And Shells Exhibiting Geometric Non-Linear Behaviour – NAFEMS 1993 – Ref. : R0029

[13] Franssen J.M. and Al.. – A Comparison Between Five Structural Fire Codes Applied To Steel Elements – IAFSS, Fire Safety Science, Proceedings Of the Fourth International Symposium.